Observation of Fine Structures in Laser-Driven Electron Beams Using Coherent Transition Radiation

Y. Glinec,[1] J. Faure,[1] A. Norlin,[1] A. Pukhov,[2] and V. Malka[1,*]

[1]*Laboratoire d'Optique Appliquée - ENSTA, UMR 7639, CNRS, École Polytechnique, 91761 Palaiseau, France*

[2]*Institut fuer Theoretische Physik I, University of Duesseldorf, 40225 Duesseldorf, Germany*

(Received 21 August 2006; published 9 May 2007)

We have measured the coherent optical transition radiation emitted by an electron beam from laser-plasma interaction. The measurement of the spectrum of the radiation reveals fine structures of the electron beam in the range 400–1000 nm. These structures are reproduced using an electron distribution from a 3D particle-in-cell simulation and are attributed to microbunching of the electron bunch due to its interaction with the laser field. When the radiator is placed closer to the interaction point, spectral oscillations have also been recorded, signature of the interference of the radiation produced by two electron bunches delayed by 74 fs. The second electron bunch duration is shown to be ultrashort to match the intensity level of the radiation. Whereas transition radiation was used at longer wavelengths in order to estimate the electron bunch length, this study focuses on the ultrashort structures of the electron beam.

DOI: 10.1103/PhysRevLett.98.194801 PACS numbers: 29.27.Fh, 52.38.Kd

Transition radiation is widely used to diagnose electron beams [1]. This radiation is emitted by a charged particle at an interface, where the dielectric function varies [2,3]. This technique is now used with thin metallic foils in particle accelerators and carries information on the electron beam distribution such as the beam energy and the angular spread [1], the spot size, the bunch shape [4], or its length [5]. More recently, this technique has been suggested to measure the microbunch separation (longitudinal modulation) produced in a free electron laser [6]. Microbunching has been observed in the far infrared [7] and in the visible range using coherent optical transition radiation (COTR) [8], where a strong dependency of microbunching with propagation distance in the undulators has been measured.

In laser-plasma interaction, COTR has shown the generation of bursts of electrons at the second harmonic of the laser on a solid target [9]. In underdense interaction for electron acceleration, transition radiation has been recorded at different wavelengths to retrieve information on the envelope of the electron beam. In the range 0.1–1 mm [10,11], it has shown the production of a bright THz source, adapted to applications. The authors concluded that their measurement was consistent with sub-100 fs electron bunches. The issue was also addressed in the range 8–10 μm [12].

Transition radiation can give useful information on the electron bunch temporal structures when the radiation is coherent or partially coherent. The radiation is usually said to be incoherent when the bunch size is longer than the emitted wavelength: electrons generate transition radiation at random phases and the radiated fields do not add up coherently. On the other hand, when the bunch contains temporal structures which are shorter than the wavelength of emission, electrons radiate in phase and the radiation adds up coherently. In consequence, the radiation is coherent or at least partially coherent and it is orders of magnitude larger than the incoherent signal. In this case, the spectrum of the radiation is closely related to the Fourier transform of the bunch shape. Thus, measuring the transition radiation spectrum gives information on the bunch temporal structures.

Here, we focus on shorter wavelengths corresponding to the inner structure of the electron beam. We have recorded the optical transition radiation (OTR) radiation emitted by the electron beam at an interface in the visible range. First, we show that the radiation intensity measured drops dramatically as the distance to the radiator increases, showing the coherence properties of the emission. A simultaneous measurement of the radiation spectrum at different distances reveals peaks and rapid spectral modulations, showing structures of the electron beam accelerated using a laser-plasma accelerator. An electron beam from a particle-in-cell (PIC) simulation is used to compute the OTR radiation, which successfully reproduces spectral peaks and confirms the interpretation proposed.

The experiment is performed on the Ti:sapphire laser in ''salle jaune'' at Laboratoire d'Optique Appliquée (LOA), which operates in chirped-pulse amplification mode at 820 nm [13]. The laser delivers 30 fs at full width at half maximum (FWHM) linearly polarized pulses with on-target energies of 1.1 J. The laser beam is focused with an $f/18$ off-axis parabolic mirror onto a sharp-edged, constant density profile, 3 mm-diameter supersonic helium gas jet, which provides an initial plasma electron density n_e of 5.0×10^{18} cm^{-3}. The waist of the focal spot is 18 μm, resulting in vacuum focused intensities of the order of 3.6×10^{18} W/cm^2, which corresponds to a normalized laser vector potential, $a_0 = eA/m_e c^2$, of 1.3.

At the interaction point, the large ponderomotive force of the laser expels the electrons from the propagation axis. This drives a nonlinear plasma wave behind the laser pulse, corresponding to a peak longitudinal electric field of the

order of 1 TV/m. Electrons from the plasma are self-injected in this structure and accelerated to high energies (~ 200 MeV) over a few millimeters [14,15]. The structure of this electron beam is analyzed using forward OTR diagnostic. A 100 μm-thick aluminum foil is placed on the electron path and the radiation generated at its boundary is simultaneously (using a glass window) imaged onto a 16-bit charge coupled device (CCD) camera and onto the slit of an imaging spectrometer in the visible range. This spectrometer contains a grating with 150 lines per millimeter, blazed at 500 nm. The instrumental response of the CCD camera, the spectrometer, and the density filters have been absolutely calibrated and corrections have been applied on the spectra shown here. The spectral range of detection is limited to 400–1000 nm. Between shots, the aluminum foil is moved laterally to a clean surface. Null tests were performed without gas to check that no signal was recorded. This relatively thick foil ensures opacity to both the amplified spontaneous emission and the main laser pulse.

Figure 1 shows the OTR energy emitted in the range 400–1000 nm for different positions of the radiator (1.5 mm, 30 mm, and 140 mm). The integrated number of counts of the OTR images on the CCD camera have been converted into emitted energy using the absolute calibration of the detection system. Independent electron spectra have been obtained using a magnet and the absolute calibration of a scintillator screen [16]. The estimated level of incoherent OTR radiation for these spectra is represented by a gray area. At the shortest distance, the energy emitted is about 5 orders of magnitude higher than this incoherent level and the signal remains above this level even at 140 mm, revealing the partially coherent nature of the emission.

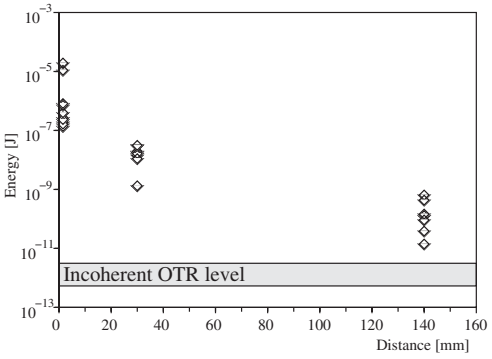

FIG. 1. OTR energy in the range 0.4–1.0 μm from the imaging diagnostic as function of the position of the radiator. After correction for the background, the signal has been integrated over the CCD chip and converted into energy using the absolute calibration of the detection system (spectral response from the CCD and the filters). The gray area represents the energy level for an incoherent emission estimated using the electron spectra measured independently.

As the radiator is placed further along the laser axis, the optical diagnostic is moved to keep the collection angle constant. The closer the radiator, the more intense the radiation. The decrease of OTR intensity comes from (i) the increasing size of the emitting area because of the divergence of the beam, (ii) the smoothing of the structures of the electron beam upon propagation due to the distribution of longitudinal and transverse momenta, and (iii) the space-charge effect. And also because of the scattering in the foil itself, it is not expected to have a fully coherent emission at the exit plane of the radiator. However, the level of OTR energy emitted, its dependence with distance and the fluctuations of the signal (well above the usual charge fluctuations) are evidence of the partially coherent emission of radiation. Thus, this electromagnetic wave contains information about the delay between electrons at the interface for the fraction of electrons which contributes to this intense signal. The spectral properties of the OTR radiation are shown hereafter.

Now, the radiator is placed at 30 mm from the interaction point. Figure 2 shows two examples of OTR spectra with peaks at different wavelengths (430, 570, 590, and 740 nm). For these shots, an iris was used which limited the half angle of collection to 3 and 8 mrad, respectively, for spectra (a) and (b). On curve (a), the signal rises again above 800 nm. This particular feature, for which the sensitivity of the detector drops, depends on the background substraction. However, the spectral response is flat in the range 450–680 nm and other peaks are not artifacts.

In our usual experimental conditions, the laser pulse is shorter than the plasma period and it self-shortens during the interaction [17]. Therefore, the electrons are injected in the plasma wave, where the electric field of the laser is weaker. As the electrons dephase with respect to the plasma wave during their acceleration, the most energetic ones will experience the strong transverse electric field of the laser, which will modulate the electron beam. It is

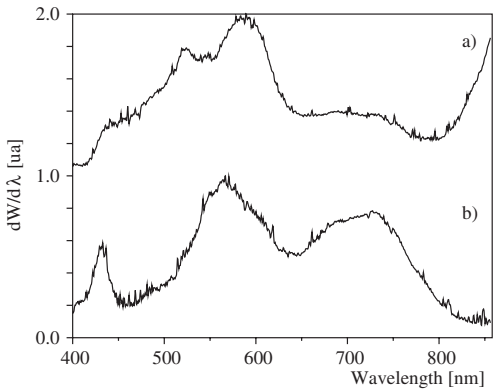

FIG. 2. Examples of OTR spectra obtained experimentally for a radiator placed at 30 mm from the interaction point. These spectra are deconvolved from the instrumental response. An iris limits the collection angle to half angles of (a) 3 mrad and (b) 8 mrad.

likely that these peaks in the OTR spectra are the signature of the interaction of the electron beam with the back of the laser pulse, which has been reported recently by measuring the correlation between the electron bunch ellipticity and the polarization of the laser [18].

One also notices that the wavelengths of the peaks differ from the central wavelength of the laser (about 810 nm). In fact, the plasma wave and the relativistic self-phase modulation modify the laser wavelength during its propagation. In our extremely nonlinear conditions, this leads to a blueshift of the laser frequency at the back of the laser pulse [17], where the electrons are. This explains the short wavelength of modulations in the experimental observations.

In order to confirm this point, the transition radiation has been computed using an electron distribution from a 3D PIC code which reproduces the typical experimental conditions. This simulation, performed with parameters similar to our experimental conditions, has been described in detail in Ref. [14]. The electron distribution is shown in Fig. 3. In the simulation, we have considered only the most energetic electrons (above 100 MeV, corresponding to 150 000 particles) in order to limit the computation time. These energetic electrons will emit in a cone with half angle $1/\gamma \sim 5$ mrad, which agrees with the collection angle in Fig. 2. Here, the spectrum has been computed after a propagation of only 100 μm because in the simulation, the transition becomes quickly incoherent owing to the small number of electrons that were used for the calculation compared to the experiments. There are some other reasons that might also explain a more intense OTR signal in the experiments even for larger distances (see Fig. 1): (i) the less energetic part of the distribution is more sensitive to the laser field, more easily modulated, and their contribution to the spectral peak in the OTR might be large; (ii) after they exit the plasma, the electrons remain under the influence of the laser field over a distance comparable to the Rayleigh length $Z_r \sim 1.4$ mm (natural diffraction length).

There are different theories on the OTR radiation emitted by an electron at a metal-vacuum interface. We have used separately the angular distribution [19,20] and the spatial distribution [21] of the radiation, the latter assuming an electron incidence perpendicular to the radiator. From Ref. [21], only the part of the electric field which propagates up to the detector has been simulated. The electric field has been summed over the electron distribution. Each contribution includes a phase which takes into account the delay for the radiation to be emitted (containing longitudinal and transverse momenta of the electrons) and the delay due to the geometry of observation.

The computed spectra are shown in Fig. 4. Both methods give similar spectrum with similar intensity. The mismatch comes from the assumptions of the two models. One notices a peak around 600 nm, corresponding to wavelength of the spatial modulations seen in Fig. 3. This modulation is the result of the interaction with the electric field of the laser, blueshifted by nonlinear effects. One also notes the second harmonic in the computed spectrum. This second harmonic could not be observed in the experiment due to a lack of sensitivity at this wavelength.

The radiator has also been placed closer to the electron source at $L = 1.5$ mm from the output of the gas jet. Figure 5(a) reveals very interesting features: well-defined spectral modulations of the OTR spectrum. This interference pattern is produced by two successive electron bunches separated by a delay τ, which will modulate the spectrum with a phase $\omega\tau$, where ω is the pulsation of the radiation from the spectrum. From the period of the modulations in the range 500–600 nm, one obtains a delay $\tau = 74$ fs. Using scintillator screens to observe the transverse electron beam profile, we have already seen several electron bunches in the same shot [22]. The effects of beam propagation up to the radiator (different average kinetic

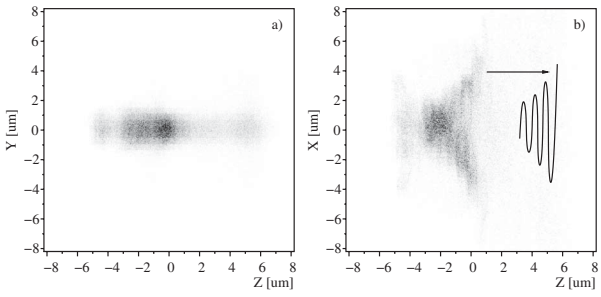

FIG. 3. Electron distribution from 3D PIC simulation, containing electrons above 100 MeV: (a) perpendicular to the plane of polarization of the laser, (b) in the plane of polarization of the laser. The electrons move from left to right. A structure in the electron distribution can be seen as the electrons overlap with the transverse laser field. This structure is reproduced with a solid line shifted to the right.

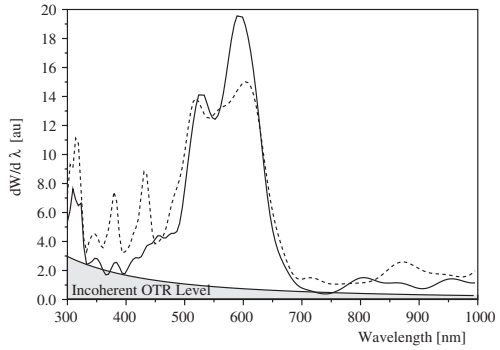

FIG. 4. OTR spectrum generated at a metal-vacuum boundary placed at 100 μm from the electron distribution in Fig. 3, using the angular distribution (solid line) and the spatial distribution (dashed line). The ratio between the coherent peak and the incoherent level scales linearly with the number of particles (150 000 electrons are used in the simulations).

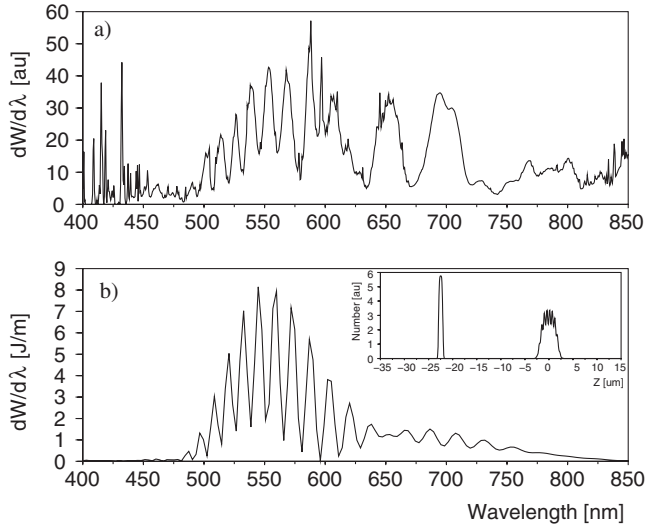

FIG. 5. (a) OTR spectrum with high frequency modulations in the range 500–600 nm. The very high frequency signal below 450 nm contains only noise from x rays directly detected by the CCD camera. The half angle of collection is 70 mrad. (b) Example of OTR spectrum computed using two electron bunches, as shown in the inset.

energy or output angles) cannot explain alone the large delay measured.

Therefore, the two electrons beams are expected to have an initial separation and to originate from two different (successive) plasma wave buckets. The linear plasma period $\tau_l = 50$ fs is slightly lower than the observed delay. But in such nonlinear interaction, the plasma period might be longer than the linear case due to the relativistic factor of the electrons or the beam loading (saturation of charge). The geometrical effects described before may also account for a small additional delay. From the expression of the nonlinear plasma period, one can estimate the maximum relativistic factor of the electrons contributing to the plasma wave $\gamma_e = (\tau/\tau_l)^2 = 2.3$ by neglecting all other contribution to the measured delay.

The main features of the observed spectrum in Fig. 5(a) are reproduced in Fig. 5(b) using the temporal profile shown in the inset. The first pulse is modulated at 550 nm by the laser pulse in order to produce a peak in the radiation spectrum. The second bunch delayed by 75 fs is not under the influence of the laser. It creates a broadband OTR spectrum over the optical wavelengths which interferes with the peaked spectrum generated by the first bunch. There are various realistic temporal profiles that allow to reproduce the observed modulations. Here, it is assumed that both electron bunches have the same electron spectrum corresponding to a measured one. The first and second bunches, respectively, contain 70% and 30% of the charge and have a duration of 10 fs and 3 fs (FWHM). Because the second electron bunch is not expected to be modulated, a fundamental result is the requirement of an ultrashort bunch duration (a few femtoseconds) in order to reproduce the signal level obtained in Fig. 1.

In conclusion, optical transition radiation has been applied to laser-plasma based electron beams to diagnose the fine temporal structures of the electron beam. This radiation reveals the modulations of the electron beam by the intense blueshifted electric field of the laser. The emission loses coherence as the radiator is placed further away from the interaction point. The electron beam structure can even be more complex and can produce spectral interferences in the OTR signal coming from two electron bunches. This technique has shown the acceleration of two electron bunches in two successive plasma wave buckets. The level of OTR signal recorded in the experiments suggests an ultrashort electron bunch duration (a few femtoseconds).

The authors would like to acknowledge fruitful discussions with W. P. Leemans and P. Muggli and a special thanks to A. H. Lumpkin for all his suggestions.

*Electronic address: victor.malka@ensta.fr

[1] L. Wartski, S. Roland, J. Lasalle, M. Bolore, and G. Filippi, J. Appl. Phys. **46**, 3644 (1975).
[2] V. Ginzburg and I. Frank, Zh. Eksp. Teor. Fiz. **16**, 15 (1946).
[3] P. Goldsmith and J. Jelley, Philos. Mag. **4**, 836 (1959).
[4] Y. Shibata *et al.*, Phys. Rev. A **45**, R8340 (1992).
[5] P. Kung, H.-C. Lihn, H. Wiedemann, and D. Bocek, Phys. Rev. Lett. **73**, 967 (1994).
[6] J. Rosenzweig, G. Travish, and A. Tremaine, Nucl. Instrum. Methods Phys. Res., Sect. A **365**, 255 (1995).
[7] A. Tremaine *et al.*, Phys. Rev. Lett. **81**, 5816 (1998).
[8] A. Lumpkin *et al.*, Phys. Rev. Lett. **88**, 234801 (2002).
[9] S. Baton *et al.*, Phys. Rev. Lett. **91**, 105001 (2003).
[10] W. Leemans *et al.*, Phys. Plasmas **11**, 2899 (2004).
[11] J. van Tilborg *et al.*, Phys. Rev. Lett. **96**, 014801 (2006).
[12] J. Faure, Y. Glinec, G. Gallot, and V. Malka, Phys. Plasmas **13**, 056706 (2006).
[13] M. Pittman, S. Ferré, J.-P. Rousseau, L. Notebaert, J. P. Chambaret, and G. Chériaux, Appl. Phys. B **74**, 529 (2002).
[14] J. Faure *et al.*, Nature (London) **431**, 541 (2004).
[15] V. Malka *et al.*, Science **298**, 1596 (2002).
[16] Y. Glinec *et al.*, Rev. Sci. Instrum. **77**, 103301 (2006).
[17] J. Faure *et al.*, Phys. Rev. Lett. **95**, 205003 (2005).
[18] S. Mangles *et al.*, Phys. Rev. Lett. **96**, 215001 (2006).
[19] C. B. Schroeder, E. Esarey, J. van Tilborg, and W. P. Leemans, Phys. Rev. E **69**, 016501 (2004).
[20] M. Ter-Mikaelian, *High Energy Electromagnetic Processes in Condensed Media* (Wiley-Interscience, New York, 1972).
[21] M. Castellano and V. Verzilov, Phys. Rev. ST Accel. Beams **1**, 062801 (1998).
[22] Y. Glinec *et al.*, Laser Part. Beams **23**, 161 (2005).